

Simulation and Experimental Study on Influence of Flow Field Parameters on Electrochemical Machining Performance

Wangwang Chen, Zhenghui Ge*, Yongwei Zhu, Yuan Hou

College of Mechanical Engineering, Yangzhou University, Yangzhou, China

*E-mail: zhge@yzu.edu.cn

Received: 30 April 2022 / Accepted: 24 June 2022 / Published: 7 August 2022

In electrochemical machining (ECM) processes, flow field parameters are closely related to the distribution of machined product such as bubbles and Joule heat in the inter-electrode gap. Therefore, the flow field is usually regarded as the key factor for achieving better surface quality and machining efficiency during ECM processes. In this study, a multi-physics model combining the electric field, the two-phase flow field and temperature field was developed. The changes in the bubble volume fraction and the flow rate in the inter-electrode gap for different flow field parameters were simulated and analyzed by COMSOL simulation software. The results show that the flow rate increases significantly with increases in the inlet pressure. Changing the outlet cross-sectional area significantly impacts the bubble volume fraction and the flow rate of the machining area. After a certain proportion of the outlet cross-sectional area, the bubble volume fraction and the flow rate in the gap change significantly. In addition, increasing the static pressure is conducive to compressing the bubble volume in the machining gap. Experiments were also performed, and the results show that as the inlet pressure increases, the material removal rate (MRR) first increases and then tends to be stable. Reducing the outlet cross-sectional area can improve the MRR and surface quality, and the machining performance is the best when the outlet cross-sectional area is 50 degrees.

Keywords: electrochemical machining; flow field parameters; multi-physics model simulation; experiment

1. INTRODUCTION

Electrochemical machining (ECM) is a manufacturing technology based on the mechanism of anodic dissolution during an electrolysis process. ECM is superior to other traditional machining processes in many aspect, such as its higher material removal rate (MRR), better surface quality, no residual stress, and no tool wear, which present obvious technical advantages for machining difficult-to-cut materials [1–2]. In ECM processes, the flow field parameters are linked to the removal of machined products. The distribution morphologies and removal of machined products, such as bubbles

and Joule heat generated by the ECM, significantly affect the current density distribution on the anode surface. Therefore, the flow field parameters are regarded as the key factors for improving the material MRR and surface quality during ECM [3–4].

Many research studies have been conducted by domestic and foreign scholars regarding flow field parameters during electrochemical machining. Some scholars focused on the influence of fluid parameters on the electrochemical machining performance. Qu et al. showed through a simulation experiment that progressive-pressure electrolyte flow could produce a higher electrolyte flow rate in the inter-electrode gap. The experiment proved that progressive-pressure electrolyte flow could provide a higher cathode feed rate under processing conditions that require a large feed. The surface roughness of the convex part, concave part, and hub of the channels was reduced and the machining accuracy of the hub was enhanced [5]. Fang et al. presented a multi-physics model that combined electrical, thermal, dilute material transport and fluid flow, and conducted an ECM simulation study using pulsating flow. Their experiment confirmed that the pulsating flow parameters were beneficial for improving the material MRR and surface quality of the workpiece [6]. Chen et al. conducted a multi-physics simulation experiment based on an electric field, a two-phase flow field, and a temperature field, and discussed the numerical simulation results for the gas volume fraction, the temperature, and the conductivity in the equilibrium state. The experiment proved that the optimized flow field parameters could significantly improve the machining accuracy of the workpiece contour [7].

Liu et al. found that changing the style of the internal flow channel of the tool electrode could control the electrolyte flow direction in the machining area; on this basis, stray corrosion were reduced and the surface quality of a TB6 titanium alloy workpiece was improved [8]. Yue et al. increased the electrolyte flow rate in the edge region and decreased it in the middle region by adding the electrolyte outlet at the bottom of the tool electrode, thereby improving the forming accuracy of an anode workpiece [9]. Chai et al. simulated and analyzed the hydrogen volume fraction and electrolyte temperature field using the gas-liquid two-phase flow theory and the convective heat transfer mathematical model. They found that when only the processing voltage or the electrolyte inlet pressure changed, among all the factors affecting the processing, the electrolyte temperature played a leading role. When only the electrode feed rate changed, the hydrogen volume fraction is the most important factor [10].

Another part of scholars focused on the influence of flow field mode on electrochemical machining performance. Xu et al. used I shape flow mode to process blisk cascade passages. Compared with the traditional lateral flow mode and positive flow mode, it was proved that the flow field was more uniform by using type I flow mode, which could significantly improve the processing quality and efficiency [11]. Zhu et al. proposed a new dynamic additional electrolyte flow mode for the local poor fluid regions, and obtained a uniform flow field by optimizing the additional pressure of the flow mode. Finally, the experiment proved that the process method can greatly reduce the surface roughness of the hub [12]. Wang et al. used a mask with a cone-shaped holes to improve the electrolyte flow when machining the hole array by mask electrochemical machining. Through simulation and experiment, it was found that when the mask wall angle was 140 degrees, the machining accuracy of the hole was stably improved [13]. Li et al. for counter-rotating electrochemical

machining, propose a new flow mode that flowing into the processing zone from both sides and top of the fixture and then flowing out from the bottom, and make the velocity distribution more uniform. The experimental results show that the method can realize stable machining process under small gap conditions and significantly improve the accuracy of ECM [14]. Ren et al. proposed a new electrolyte flow mode with auxiliary internal fluid. By apply supplementary electrolyte in the machining area, the flow field uniformity was significantly improved, and the experiment proved that the machining accuracy of grid structure workpiece was effectively improved under this flow mode [15]. Guo et al. for the processing quality of the leading edge and trailing edge, a new blade flow mode with independent electrolyte supply at the leading edge and trailing edges of the blade to improve the flow field uniformity in the edge area of the blade was proposed [16]. Gu et al. propose forward flow field mode and the lateral flow field mode, and establish the numerical models for them separately. The experiment and simulation proved that, in forward flow field mode, can make higher flow rate, and feed speed is batter. In lateral flow field mode, can make more uniform flow rate, the machining quality is greatly improved [17].

In summary, during ECM, the flow field parameters affect the material MRR and the surface quality of an anode workpiece. In this study, a multi-physics model simulation was performed to determine the changes in the bubble volume fraction and the flow rate in the flow channel under different flow field parameters. The influence of the flow field parameters on the ECM was systematically analyzed through experiments, and the optimal ECM machining conditions were summarized for different flow field parameters.

2. THEORETICAL MODEL

2.1 Electric field model

In this paper, the influence of different flow field parameters on ECM in a closed flow channel is studied. The model is shown in Fig. 1, the potential distribution of electrolyte is given by the law of charge conservation:

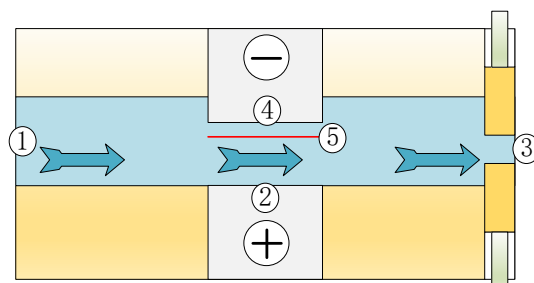


Figure 1. Geometric model of ECM process

$$\nabla^2\varphi=0 \tag{1}$$

The boundary conditions are as follows: ① is the fluid inlet and ③ is the adjustable fluid outlet $\varphi_2=U$, $\varphi_4=0$, Take the data on line ⑤ as the research object.

Temperature and bubble rate directly affect the conductivity of electrolyte, the continuity equation is

$$K=K_0[1+\zeta(T-T_0)](1-\beta)^m \quad (2)$$

where K_0 is the initial conductivity, ζ is the temperature coefficient, T_0 is the initial temperature, β is the bubble rate, and m is the bubble influence index.

Assuming that only the cathode generates hydrogen in ECM, the amount of hydrogen generated by the cathode per unit time and unit area can be expressed as: [18]

$$M_H = k_H I \quad (3)$$

where M_H is the mass of hydrogen generated, k_H is the electrochemical equivalent of hydrogen, can be described as:

$$k_H = \frac{M}{2F}$$

where M is the atomic mass of the element and F is the Faraday constant; I is the current density.

2.2 Two-phase turbulent flow model

In ECM, the flow channel should be contains dissolved metal, gas and liquid, which is a three-phase flow. Due to the small proportion of dissolved metal. The influence of dissolved metal on the process of ECM is ignored in this paper.

In this paper, Euler-Euler model is used to study the distribution of bubble rate and velocity in the inter-electrode gap. The two-phase turbulent model in ECM meets the momentum equations[18], that is:

$$\tilde{\rho}_g \left[\frac{\partial \mu_g}{\partial t} + u_g \nabla u_g \right] = -\beta_g \nabla p + \nabla \tau_g + \tilde{\rho}_g g + F_m \quad (4)$$

$$\tilde{\rho}_l \left[\frac{\partial \mu_l}{\partial t} + u_l \nabla u_l \right] = (1-\beta_l) \nabla p + \nabla \tau_l + \tilde{\rho}_l g - F_m \quad (5)$$

where the subscripts “g” and “l” represent the amount related to gas phase and liquid phase, β_g is the proportion of gas in gas-liquid two phases; β_l is the proportion of liquid in gas-liquid two-phase; ρ_g and ρ_l are gas and liquid density respectively; u_g and u_l are gas and liquid velocities, respectively; p is pressure, and τ_l is viscous stress tensor.

The electrolyte in inter-electrode gap is turbulent, so k- ε [19] turbulence model is used in this paper. The transport equations of turbulent kinetic energy and turbulent dissipation rate are given by:

$$\frac{\partial(\rho k)}{\partial t} + \frac{\partial(\rho k u_j)}{\partial x_j} = \frac{\partial}{\partial x_j} \left[\left(\mu + \frac{\mu_T}{\sigma_k} \right) \frac{\partial(\rho k)}{\partial x_j} \right] + \rho(P_k - \varepsilon) \quad (6)$$

$$\frac{\partial(\rho \varepsilon)}{\partial t} + \frac{\partial(\rho \varepsilon u_j)}{\partial x_j} = \frac{\partial}{\partial x_j} \left[\left(\mu + \frac{\mu_T}{\sigma_\varepsilon} \right) \frac{\partial \varepsilon}{\partial x_j} \right] + \rho C_1 E \varepsilon - \rho C_2 \frac{\varepsilon^2}{k + \sqrt{v \varepsilon}} \quad (7)$$

where the k is turbulent kinetic energy; ε is turbulent dissipation rate; μ is molecular viscosity coefficient; μ_T is turbulent eddy viscosity coefficient; ρ is electrolyte density; x_j is the coordinate

component; u_j is the average relative velocity component; P_k is the turbulent kinetic energy generation term.

$$C_1 = \max(0.43, \frac{\eta}{\eta+5}) \quad (8)$$

$$C_1 = \frac{1}{A_0 + A_5 U^* K / \varepsilon} \quad (9)$$

$$A_5 = \sqrt{6} \cos \Phi \quad (10)$$

$$\Phi = \frac{1}{3} \cos^{-1}(\sqrt{6}W) \quad (11)$$

$$W = \frac{E_{ij} E_{jk} E_{ki}}{(E_{ij} E_{ij})^{\frac{1}{2}}} \quad (12)$$

η is current efficiency, Φ is filtering scale; E_{ij} is the mainstream time-averaged strain rate; C_1 , C_2 , A_0 are model constants.

2.3 Thermal model

The temperature change in the inter-electrode gap is calculated by the convection-diffusion equation[20]:

$$\rho c_p \frac{\partial T}{\partial t} + \rho c_p u \nabla T = \nabla(\lambda \nabla T) + Q \quad (13)$$

where the c_p is the specific heat capacity, u is the flow rate, ∇ is the differential operator, λ is the electrolyte thermal conductivity, Q is the Joule heat generated by the inter-electrode gap, and the calculation equation is:

$$Q = EI \quad (14)$$

where the E is the electric field intensity gradient.

The convective heat flux on cathode and anode surface is:

$$q = h(T_1 - T_2) \quad (15)$$

where the q is convective heat flux, h is heat transfer coefficient, T_1 and T_2 are boundary temperature of cathode and anode, respectively.

2.4 Reactant transport model

In ECM, the products are metal ions of the anodic dissolution, hydrogen and oxygen generated by anode and cathode respectively. The transmission of reactants in the inter-electrode gap is mainly migration, convection and diffusion. The main transport mechanism of the anode–electrolyte layer is diffusion.

The governing equations based on Fick diffusion law and forced convection of fluid flow are

given by:

$$\frac{\partial C_i}{\partial t} + \nabla(C_i u - D_i \nabla C_i + D_i N_i) = 0 \quad (16)$$

where C_i denotes the dilution concentration of diluted species i , D_i denotes the diffusion coefficient of diluted species i and N_i denotes the flux of diluted species i .

3. SIMULATION RESULTS

COMSOL software was used to simulate the evolution of process variables such as bubble rate and fluid velocity in ECM. All simulations were carried out in the transient mode with zero initial expression.

3.1 Effect of different inlet pressures on flow field

Multi-physics model simulations were conducted with different inlet pressures when processing voltage was 20 V and the outlet was fully open. The flow rate variation in the inter-electrode gap is shown in Fig. 2. The figure shows that the flow rate increases with the inlet pressure, and that the change is particularly obvious at low inlet pressures. When the inlet pressure is 4 MPa, the flow rate is approximately 50m/s, and when the inlet pressure is 0.5 MPa, the flow rate is approximately about 15 m/s. Variance is used to describe the discrete degree of a set of data.

Fig. 3 presents the flow rate Variance for each inlet pressure. The figure shows that, variance is nearly proportional to the increase in the inlet pressure.

This indicates that, the flow rate increases with inlet pressure; meanwhile, the flow field also show a more disordered trend, which promotes the removal effect of machined products in the inter-electrode gap.

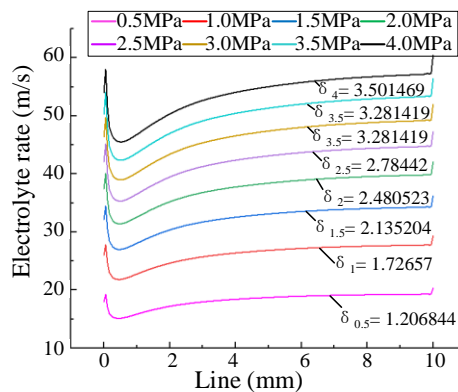


Figure 2. Flow rate Variation at different inlet pressures

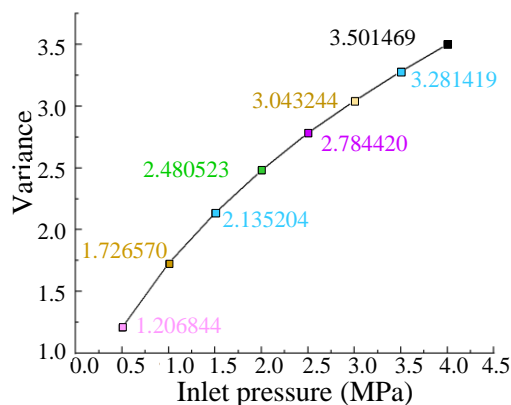


Figure 3. Flow rate Variation at different inlet pressures

Fig. 4 shows the bubble volume fraction distribution in the inter-electrode gap at different inlet pressures. With inlet pressure increases, the bubble volume fraction decreases. This could increase the conductivity in the inter-electrode gap and is beneficial for obtaining higher current densities. Therefore, increasing the inlet pressure is conducive to improving the processing efficiency and obtaining better surface quality during ECM.

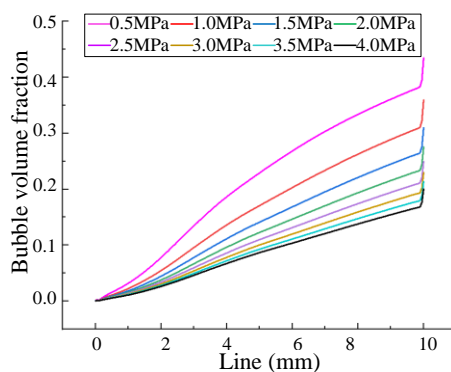


Figure 4. Bubble volume fraction Distribution at different inlet pressures

3.2 Effect of different outlet cross-sectional area on flow field

Multi-physics model simulations were performed with different outlet cross-sectional area proportions when processing voltage was 20 V and inlet pressure was 2 MPa. Fig. 5 shows the flow rate variation for different outlet cross-sectional area proportions. The flow rate decreases gradually as the outlet cross-sectional area decreases, and the changes are obvious when the outlet cross-sectional area proportion is low. Fig. 6 depicts the flow rate variance at different outlet cross-sectional areas. The figure shows that the variance decreases gradually with decreases in the outlet cross-sectional area; additionally, the degree of flow rate discretization in the flow channel decreases, which is not conducive to removing machined products.

Meanwhile, decreases in the variance improve the uniformity of the velocity. This has also been preliminarily verified in experiments, such as that Xu et al., who found that an outlet-cornered flow field can make the velocity more uniform [21].

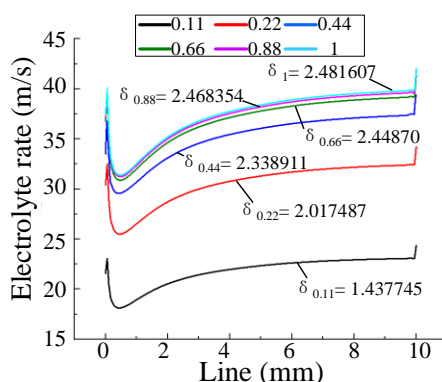


Figure 5. Flow rate variation at different outlet cross-sectional area proportions

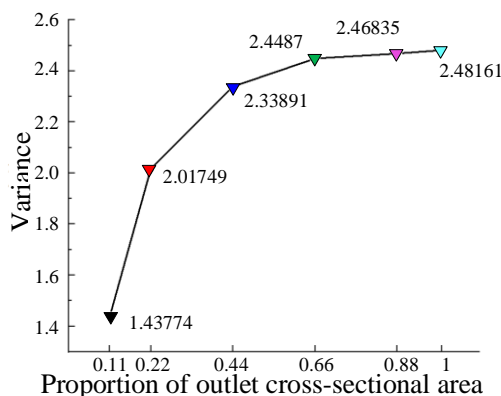


Figure 6. Variance Variation at different outlet cross-sectional area proportions

Fig. 7 presents the bubble volume fraction distribution in the inter-electrode gap at different outlet cross-sectional area proportions. The figure shows that the bubble volume fraction in the inter-electrode gap gradually increases with the decrease of outlet cross-sectional area, and when the outlet cross-sectional area is small, the bubble volume fraction increases more dramatically. Bubbles in the inter-electrode gap have a scraping effect on the wall when the fluid is turbulent, which can promote the removal of machined products from viscous layer [22]. Therefore, when the bubble volume fraction is large, deposited machined products are destroyed and easily removed in time. Meanwhile, decreases in the of outlet cross-sectional area lead to decreases the flow rate dispersion, and the removal of machined products is inhibited (as show in Fig. 6). In summary, there may be an optimized

range of outlet cross-sectional area values that can enhance removal of machined products.

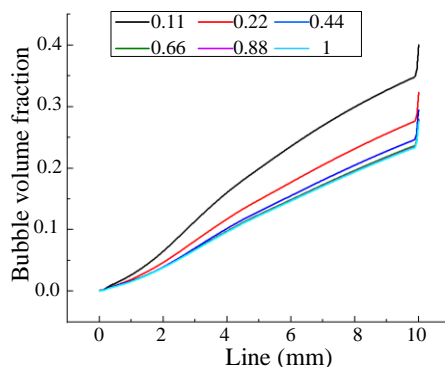


Figure 7. Bubble volume fraction distribution at different outlet cross-sectional area proportions

3.3 Effects of different static pressures on flow field

Multi-physics model simulations were performed for different static pressures when the outlet cross-sectional area proportion was 0.66, and the inlet and outlet pressures were increased synchronously to ensure that the difference between the inlet and outlet pressures remind constant at 5 MPa. The bubble volume fraction distribution for different static pressures is shown in Fig. 8. A local amplification diagram shows that the bubble volume fraction decreases with increases in the static pressure when the difference between the inlet and outlet pressures remind constant. Because the pressure difference between the inlet and outlet is invariant, the uniformity of the flow field is remains nearly unchanged. Therefore, it can be speculated that increasing the static pressure restricts the bubble volume fraction and produces a higher current density with an unchanged flow rate, which is conducive to improving the surface quality of an anode workpiece.

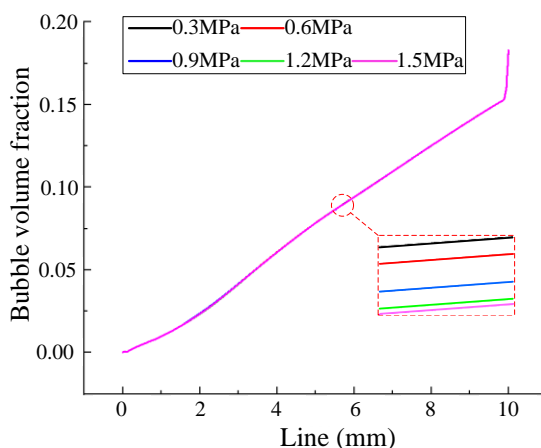


Figure 8. Bubble volume fraction Distribution at different static pressure

4. EXPERIMENTAL RESULTS AND DISCUSSION

Based on the simulation results, the ECM experiments were performed during this study at different inlet pressures, different outlet areas and different electrolytes. SS304 samples with the dimensions of 10 mm × 10 mm × 10 mm was prepared, and the samples were ultrasonically cleaned and weighed before and after the experiments. During the machining process, the initial machining gap was 0.3 mm and the other machining conditions show in Table 1.

Table 1. ECM experiment parameters

Parameters	Value
Electrolyte (10%)	NaCl, NaNO ₃
Electrolyte temperature (°C)	25
Electrolyte inlet pressure (MPa)	0.02–0.07
Outlet closure degree (°)	0–80
Workpiece material	SS304
Initial machining gap (mm)	0.6
Machining voltage (V)	DC 25, 20
Current (A)	5, 15, 20

4.1 Change inlet pressure

ECM experiments with different inlet pressures were conducted under machining conditions of 20 V, 25 °C and an NaNO₃ solution. The MRR at different inlet pressures is shown in Fig. 9. The figure shows that the sample MRR increases with the increases in the inlet pressure. When the inlet pressure is greater than 0.04 MPa, the MRR begins to fluctuate. This is because in the initial stage, the flow rate increases as the inlet pressure increases, meanwhile, the removal of machined products is promoted, thus improving the processing efficiency. When the flow rate increases to a certain extent, the influence of the flow rate on the removal of machined products tends to be stable, the inlet pressure continue to increase, so the processing efficiency remains nearly unchanged. Chai et al. [10] found through experiments, that increasing the inlet pressure was conducive to improving the machining accuracy of an anode surface. These results are similar to those presented in this paper. However, Chai et al. also found that continuous increases in the inlet pressure were not conducive to electrolyte renewal in the gap, and that they even formed a stagnation zone, which affected the cathode feed rate. This is quite different from the fact that when the pressure increases to a certain value, the MRR fluctuates. This fluctuation may occur because the processing object is the film cooling hole, the diameter depth was large. When the inlet pressure is too large, an eddy current is produced preventing the electrolyte renewal. The processing environment in this study did not produce such problems.

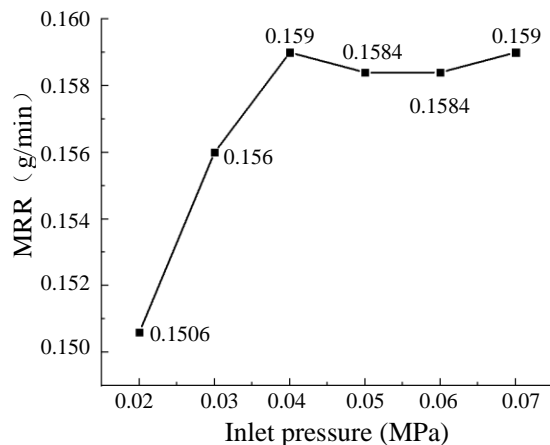


Figure 9. MRR at different inlet pressures

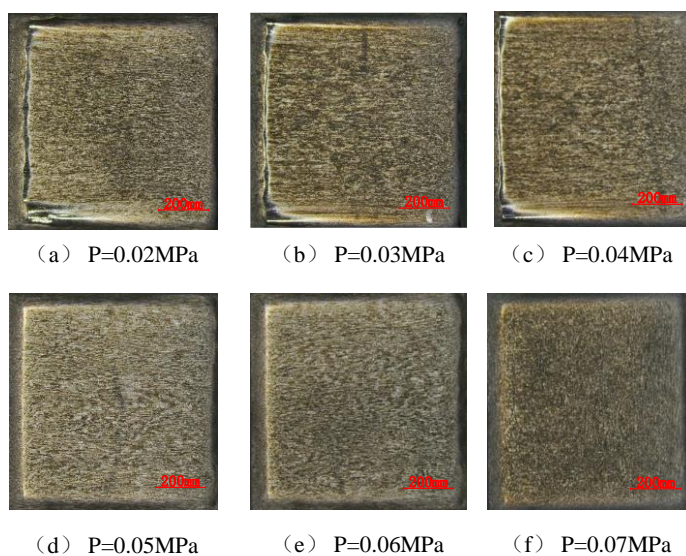


Figure 10. Samples processed under different inlet pressures.

Fig. 10 is the processing samples under different inlet pressures. When the pressure is low, the surface quality of the processing samples is poor, such as Fig. 10(a-b). This is because the low inlet pressure leads to the insufficient flow rate of electrolyte, resulting in the accumulation of machined products in the processing zone, the decrease of conductivity and the low current density on the anode surface. The surface quality of the sample is enhanced with inlet pressure increases, as shown in Fig. 10(c-f). This is because with the increase of inlet pressure, the electrolyte in high flow rate, take away the processing products quickly, the conductivity increases to ensure sufficient current density on the anode surface. meanwhile, at low pressure, there is a huge difference in the processing surface state between the inlet side and the outlet side. The surface at the inlet side is bright, and the black product near the outlet side is attached, as shown in Fig. 10(a-c). This is because in low pressure, the overall flow rate in the inter-electrode gap is insufficient, and the loss along channel makes flow rate at inlet and outlet very greatly. In contrast, at high pressure, the processing surface states of the inlet end and

the outlet are similar, as shown in Fig. 10(d-f). This is because when the pressure in high stage, the flow rate in inter-electrode gap is sufficient, and flow rate at the outlet still meet the needs of electrolytic processing after loss along channel.

4.2 Changing outlet cross-sectional area

Next, the experiments with different outlet cross-sectional areas were conducted for the machining conditions of 25 V, 25 °C and 0.05 Mpa. The influence of different outlet cross-sectional areas on the machining performance are also discussed in detail.

The MRR at different outlet cross-sectional areas is shown in Fig. 11. The figure shows that the MMR is low when the outlet cross-sectional area is 0 degrees (full open outlet). As the outlet cross-sectional area decreases, the MMR increases gradually, and the maximum MMR occurs when the outlet cross-sectional area is reduced to 50 degrees. This is because reducing the outlet area within this range leads to an electrolyte velocity decrease, but it still meets the machined products removal demand. At the same time, Simulation 3.2 (shown in Fig. 7) shows that when the outlet area decreases, an increase in the bubble volume fraction aggravates the scraping effect on the deposited machined products and the removal of machined products is promoted. The conductivity in the inter-electrode gap increases and the surface current density of the workpiece increases, and improve the processing efficiency.

However, when the outlet cross-sectional area is more than 50 degrees, the MMR has a decreasing trend, and the MMR decreases sharply when the outlet area is 80 degrees. This result occurs because the flow rate decreases rapidly in this range of outlet area reduction, and a large portion of the machined products in the flow channel cannot be effectively removed, causing a decrease in conductivity and an insufficient surface current density for the workpiece, which seriously affects the processing efficiency.

From the experimental results, the authors concluded that when the outlet cross-sectional area is approximately 50 degrees, there is an optimal matching relationship between the scouring effect of the electrolyte flow and the bubble scraping effect on the removal effect of machined products in the inter-electrode gap.

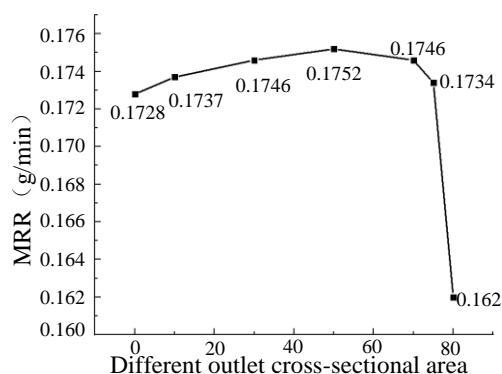


Figure 11. MRR of different outlet cross-sectional area

Fig. 12 presents a comparison of processing morphologies for different outlet cross-sectional area. When the outlet cross-sectional areas is 0 degrees, the black products of the processed sample adhere and surface quality is poor, as shown in Fig. 12(a). When the outlet cross-sectional area is 50 degrees, the machined products of the sample are removed effectively, the surface is bright, and the processing quality is significantly improved, as shown in Fig. 12(b).

These results occur because when the outlet cross-sectional area is 50 degrees, the flow rate still meets the machined products removal requirements. However, during the process of increasing the outlet cross-sectional area, the static pressure in the inter-electrode gap increases and the bubble scraping effect on the wall increases. Combined with Simulation 3.3 (as shown in Fig. 8), it is indicated that the bubble volume is compressed as the static pressure increases, which improves conductivity. These two effects demonstrate comprehensively that, when the outlet cross-sectional area is 50 degrees, the surface quality is significantly better than when the outlet is fully open.

When the outlet cross-sectional area is 80 degrees, the surface morphology of the machined surface is as shown in Fig. 12(c). The figure shows that there is an extremely uneven corrosion phenomenon on the machined surface. This occurs because when the outlet cross-sectional area is 80 degrees, the flow rate drops too much, the machined products deposit in a large number of flow channels, and the conductivity distribution on the workpiece surface is uneven, resulting in inconsistent corrosion on the machined surface.

Therefore, the authors concluded that when the outlet cross-sectional area is approximately 50 degrees, the best results are obtained for the MMR and anode surface quality, which indicates optimal processing conditions.

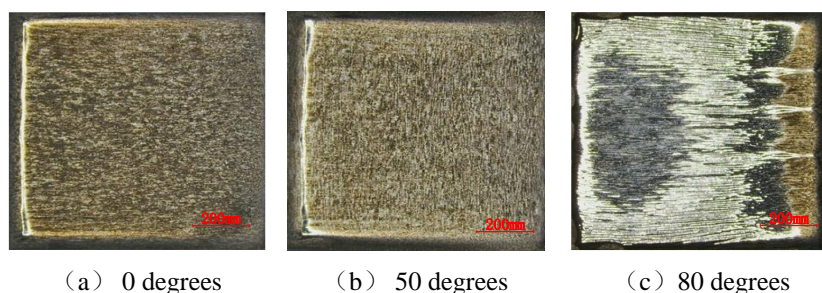


Figure 12. Processing samples with different outlet cross-sectional area

4.3 Comparison of different electrolytes

Next, the experiments with different electrolyte solutions and current densities were performed at the machining condition of 25 °C, 0.04 Mpa and fully open outlet. Fig. 13 presents a column diagram of the anode surface MRR when the electrolytes are NaCl and NaNO₃ solutions with the same parameters. The figure shows that the MRR for the NaCl solution was generally higher than that for the NaNO₃ solution. When the current is 5 A, the MRR for the NaCl and NaNO₃ solutions are 0.039 and 0.027, respectively, which represent a difference of 0.012. As the current increases, the difference

between the two gradually decreases. When current is 20 A, the MRR for the NaCl and NaNO₃ solutions are 0.1992 and 0.1956, respectively, a difference of only 0.0036. This result occurs because at low currents, the current efficiency is small because of the passivation effect of the NaNO₃ solution. With an increase in the current, the current efficiency of NaNO₃ solution increases, gradually nearing the current efficiency of the NaCl solution. Therefore, during ECM, due to the existence of NaNO₃ electrolyte passivation, NaNO₃ solution can better prevent stray corrosion and ensure the processing quality of workpiece. Pan et al. used an NaNO₃ solution during Electrochemical Micro-Machining, the machining accuracy of the micro-holes was improved, reaching 97.98 μm (front side) and 92.45 μm (back side) [23].

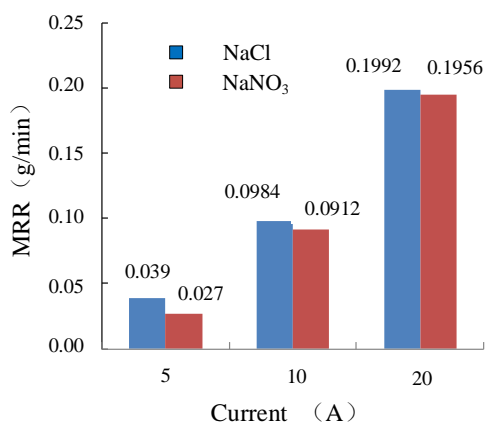


Figure 13. Comparison of the r MMR for the NaCl and NaNO₃ electrolytes

The anodic surfaces for the NaCl and NaNO₃ solutions at different currents are presents in Fig. 14. The figure shows that that when the current is 5 A, the NaNO₃-solution-machined surface has significantly more black products attach than attach to the machined surface when the electrolyte is NaCl solution. As the current increases, the difference between the amounts of black products that attach to the machined surfaces for the two electrolytes gradually decreases. When current is 20 A, there are almost no black products on the machined surfaces for the two electrolytes, and better surface quality is obtained. Meanwhile, as the current increases, the machined surface quality for the two electrolytes has an increasing trend, but the surface with the NaCl solution was invariably better than that with the NaNO₃ solution. Therefore, the NaCl solution can obtain better processing speed and surface quality than the NaNO₃ solution. Yang et al. used an NaCl solution during electrolytic machining of a metal screw pump stator. At conditions of 16 V, an electrolyte temperature of 30°, and an inlet pressure 2 MPa, a the cathode feed rate of 6 mm/min was obtained, which ensured the machining accuracy of the product [24]. Therefore, using of NaCl solutions for engineering applications is conducive to better processing efficiencies.

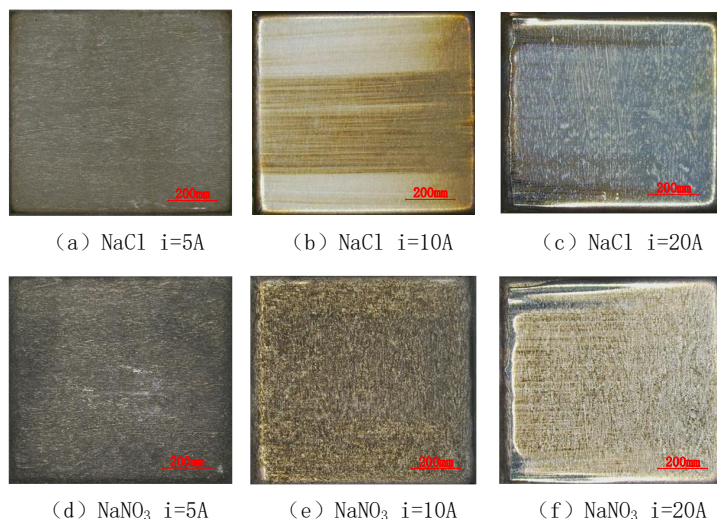


Figure 14. Surface of samples in NaCl and NaNO₃ electrolyte at different current.

5. CONCLUSION

In this paper, COMSOL software is used to simulate the multi-physics model of bubbles and velocity in flow channel under different flow field parameters. Combined with experiments, the influence of different flow field parameters on ECM performance is analyzed. The conclusions are as follows :

(1) The larger the inlet pressure is, the higher the flow rate is, and content of machined products in the inter-electrode gap decreases first and then tends to be stable. When Bubble rate decreases, the distribution of current densities on workpiece is more uniform, the replication accuracy of anode surface is improved.

(2) When outlet cross-sectional area reduced, MRR and surface quality show increase firstly and then decrease. When outlet cross-sectional area is about 50 degrees,, the highest MMR appears, and the surface quality is the best.

(3) The higher ECM voltage is, the less black products attach to sample surface are, and the brighter surface is. Moreover, the trend of change is more obvious when electrolyte is NaNO₃ solution than when electrolyte is NaCl.

ACKNOWLEDGEMENTS

The authors wish to acknowledge the financial support provided by the National Natural Science Foundation of China (52175438), Jiangsu Agricultural Science and Technology Independent Innovation Fund (CX(21)354) and Research and Practice Innovation Program for Graduate Students of Yangzhou University (SJCX21_1556).

References

1. G.X. Liu, Y.J. Zhang, W. Natsu, *Int. J. Mach. Tool. Manuf.*, 12 (2019) 66-75.

2. C.F. Zhang, P.X. Zheng, R.Y. Liang, K. Yud, X.G. Jiang, Z.H. Yan, *Int. J. Electrochem. Sci.*, 15 (2020) 1148-1159.
3. H. Zhu, C. Wang, S. Mao, Z. Zhang, D. Zhao, K. Xu, Y. Liu, L. Li, J. Zhou, *J. Manuf. Processes.*, 2022 (2022) 665-677.
4. X.C. Li, P.M. Ming, X.M. Zhang, S. Niu, X.S. Zheng, L. Yan, W. Wang, Y.Y. Zhang, *Int. J. Electrochem. Sci.*, 16 (2021) 151030.
5. N.S. Qu, Y. Hu, D. Zhu, Z.Y. Xu, *Mater. Manuf. Processes.*, 2014; 29(5):572-578.
6. X.L. Fang, N.S. Qu, Y.D. Zhang, Z.Y. Xu, D. Zhu, *J. Mater. Process. Technol.*, 214 (2014) 36-43.
7. Y.L. Chen, X.C. Zhou, P.X. Chen, Z.Q. Wang, *Chin. J. Aeronaut.*, 33(2020) 1057-1063.
8. Y. Liu, N. Qu, *Sci. China. Technol. Sci.*, 63 (2020) 2698–2708.
9. X.K. Yue, N.S. Qu, S. Niu, H.S. Li, *J. Mater. Process. Technol.*, 276 (2020) 116413.
10. M.X. Chai, Z.Y. Li, H.J. Yan, Z.X., *Int. J. Adv. Manuf. Technol.*, 112 (2021) 525–536.
11. Z.Y. Xu, L.Y. Sun, Y. Hu, J.C. Zhang, *Int. J. Adv. Manuf. Technol.*, 71 (2014) 459–469.
12. D. Zhu, J.C. Zhang, K.L. Zhang, J. Liu, Z. Chen, N.S. Qu, *Int. J. Adv. Manuf. Technol.*, 80 (2015) 637–645.
13. G.Q. Wang, H.S. Li, N.S. Qu, D. Zhu, *J. Manuf. Processes.*, 25 (2017) 246-252.
14. J.Z. Li, D.Y. Wang, D. Zhu, B. He, *J. Mater. Process. Technol.*, 275 (2020) 116323.
15. Z.Y. Ren, D.Y. Wang, G.W. Cui, W.J. Cao, D. Zhu, *Precis. Eng.*, 72 (2021) 448-460.
16. J.W. Guo, D. Zhu, Y.J. Yang, *Int. J. Adv. Manuf. Technol.*, 114 (2021) 1119–1129.
17. Z.Z. Gu, X.H. Zheng, Y.C. Ge, *Int. J. Electrochem. Sci.*, 16 (2021) 211144.
18. D.A. Drew, *Ann. Rev. Fluid. Mech.*, 15 (1983) 261–91.
19. L. Ignat, D. Pelletier, F. Ilinca, *Comput. Methods. Appl. Mech. Eng.*, 189 (2000) 1119–39.
20. Y.L. Chen, M. Fang, L.J. Jiang, *Int. J. Adv. Manuf. Technol.*, 91 (2017) 2455–2464.
21. J.W. Xu, D. Zhu, J.H. Lin, X.Y. Hu, *Int. J. Adv. Manuf. Technol.*, 107 (2020) 1551–1558.
22. Y.L. Chen, X.C. Zhou, P.Y. Chen, Z.Q. Wang, *J. Mech. Eng. Sci.*, 55 (2019) 215-221.
23. Y. Pan, L. Xu, *Int. J. Precis. Eng. Manuf.*, 16 (2015) 143–149.
24. F. Yang, T. Ren, H. Wang, H.B. Wang, B.X. Liu, M. Chen, *Int. J. Adv. Manuf. Technol.*, 89 (2017) 1317–1326.